Chemical Physics 21 (1976) 1–19

COMPUTER SIMULATION OF THE PULSED Cl + HBr CHEMICAL LASER: EFFECTS OF ROTATIONAL NONEQUILIBRIUM

E. KEREN *, R.B. GERBER and A. BEN-SHAUL
Department of Physical Chemistry, The Hebrew University, Jerusalem, Israel,
and Department of Chemical Physics, The Weizmann Institute of Science, Rehovot, Israel

Received 1 June 1976

The time evolution of the pulsed Cl + HBr chemical laser is obtained by numerical solution of the coupled master equations that describe the kinetic development of the vib-rotational species and the photon densities in that system. Special attention is given to the time evolution of the distributions of rotational populations and to its effect on the system. The main conclusions reached are:

(1) The rotational distribution function is non-Boltzmann throughout the laser pulse (except at high inert gas pressures) and has either a broad single maximum or a double hump structure.

(2) The photon densities at low J values exhibit extended oscillations following lasing threshold. At high J's the threshold oscillations are fewer and the pulse shape is typical of a nearly steady state situation.

(3) The behaviour of the laser pulse at threshold is determined largely by the pumping and radiation processes. Relaxation effects become significant only beyond threshold time.

These results can be useful for the development of approximation methods for solving the laser master equations.

1. Introduction

The intensive experimental activity in the field of molecular gas lasers has triggered off also considerable interest in theoretical investigations of such systems [1] with the aims of interpreting available experiments or of predicting and anticipating observable features in new systems. Theoretical studies in this subject are also potentially useful to investigations of chemical reaction and energy transfer mechanisms and of behaviour of systems far from equilibrium. The main device for such studies are the coupled kinetic equations that include all the variables and describe the various processes that play a role in laser operation. In a laser working on vib-rotational transitions the population of each vib-rotational level must be known as a function of time. Collisional energy exchange leads to significant population of vib-rotational levels which do not participate directly in pumping or lasing. In the kinetic master equations of the laser the populations of the various vib-rotational levels are coupled with the densities of radiations from all possible transitions, thus the total number of independent variables that must be included is very large and may easily exceed the limits of computational feasibility.

Thus, methods for reducing very drastically the dimensionality of the system must be introduced. The critical factor in the dimensionality problem is the large manifold of rotational levels. To cope with the difficulty, the rotational equilibrium assumption [1,2] has been adopted in the literature, and almost universally applied in numerical work on molecular laser systems. In this approach it is assumed that rotational relaxation is instantaneous on the time scale of the other processes in the system. The rotational levels are thus taken to be Boltzmann-distributed at each instant.

A further approximation is frequently introduced, the single line model [2]: One supposes that at any instant radiation occurs only from a single transition, the one with the highest gain. Extensive numerical studies on several chemical lasers were carried out in the framework of the above approximations [2–6]. However, the validity of the above assumptions is very much in

* Present address: Department of Chemistry, University of Illinois, Urbana, Illinois, USA.

doubt. Indeed, there is experimental evidence that they are incorrect in a substantial number of cases, especially for some low-pressure lasers [7–11].

Theoretical estimates also cast doubts on the validity of this assumption by suggesting that rotational relaxation may not be fast enough to dominate over the influence of pumping and of radiation. Thus both non-equilibrium effects due to the radiation [12,13] and to the distribution produced by the pumping [12] should be expected to persist for long time intervals. The need arises to replace the rotational equilibrium assumption by a valid physical model for dealing with the distribution of rotational levels and, consequently, to develop approximation methods for solving the master equations of the chemical laser system.

The purpose of the present article is to help in bringing in such a development by carrying out an extensive computer simulation of the Cl + HBr chemical laser system. Such a "computer experiment" must, of course, correctly reproduce the available experimental observations on the system, but it provides much more detailed information than any real experiment can be expected to give. In the numerical simulation, all variables of interest can be followed as a function of time. It is reasonable to assume that an analysis of the results so obtained may shed light on simplifying features that exist in the system, and on the possibilities of developing approximation schemes accordingly. The advantage of the Cl + HBr system for this approach is that owing to the relatively low exothermicity of the reaction and to the large rotational spacings of the HCl molecule, the number of vib-rotational species that are involved in the kinetics of the laser is managable from a computational point of view. Also, for this system there is a great deal of experimental and theoretical information on many of the rate constants involved. Unavailability of rate constants (especially for individual vib-rotational states) for the various energy transfer and reaction processes severely limits the possibility of carrying out laser simulations even for favourable cases from that point of view such as Cl + HBr. One must supplement the missing data by very simple theoretical models. It is reasonable, however, to assume that if with these model rates the simulation is capable of reproducing the results of "real" experiments on the system, then the modelling should be fairly realistic.

There have been very few studies of the above type in the literature so far [9,10,12,14,15]. These investigations clearly demonstrate the inadequacies of the rotational equilibrium assumption and of the single line model. The present article differs in emphasis from the above mentioned ones, as the main effort here is an attempt to search for simplifying features in the numerical solutions obtained, especially in the distribution of the rotational populations.

The outline of the article is as follows: Section 2 describes the kinetic equations involved and the rate constants employed. Section 3 gives a brief account of the numerical method that was used in this work to cope efficiently with the large system of stiff differential equation. Section 4 surveys the "numerical experiments" we made on the laser system, describes the results obtained, analyzes the behaviour of some variables of interest and points out, when possible, to the existences of simplifying features. Finally, section 5 comments on some future directions suggested by this work.

2. The rate equations

In order to describe the temporal evolution of the laser system we employ the rate equations approach. Since we do not assume rotational equilibrium the rate equations involve: (i) The populations (number densities), $N_{V,J} = [\mathrm{HCl}(V,J)]$ of all relevant vib-rotational levels of the lasing molecules, (ii) the photon densities ρ_ν at all the relevant vib-rotational frequencies ν, (iii) the translational (heat bath) temperature T, (iv) the concentrations of the non-lasing molecular species, i.e., HBr, Cl_2, Cl and Br. It is assumed that the system is spatially uniform so that only the time dependence of these variables has to be considered. The coupled kinetic equations are solved simultaneously subject to the appropriate initial conditions.

In a symbolic notation the rate equations are of the form

$$\mathrm{d}N_{V,J}/\mathrm{d}t = P(V,J) - D(V,J) - R(V,J), \tag{1}$$

$$\mathrm{d}\rho_\nu/\mathrm{d}t = G(\nu) - L(\nu), \tag{2}$$

where $P(V,J)$ is the rate of chemical pumping, $D(V,J)$ is the net collisional deactivation rate of $\mathrm{HCl}(V,J)$ molecules, $R(V,J)$ is the net rate of radiative transitions from V,J, $G(\nu)$ is the net gain of photons with frequency ν due to radiative processes and $L(\nu)$ is the net loss

Table 1
Major rate processes in the Cl + HBr → HCl + Br laser

(I) *Radiation*

$$HCl(V, J-1) + h\nu \rightarrow HCl(V-1, J) + 2h\nu; \quad \text{P-branch.}$$

(II) *Initiation*

$$Cl_2 \xrightarrow{\text{Flash}} 2Cl \qquad \text{(R-1)}$$

(III) *Pumping*

$$Cl + HBr \rightarrow HCl(V, J) + Br \qquad \text{(R-2)}$$

(IV) *Energy transfer*

1. V–V

a. $HCl(V, J) + HCl(m, L) \rightleftarrows HCl(V \pm 1, J') + HCl(m \mp 1, L')$ (R-3)

b. $HCl(V, J) + HBr(0, L) \rightleftarrows HCl(V-1, J') + HBr(1, L')$ (R-4)

2. V–R,T

a. $HCl(V, J) + Cl_2 \rightleftarrows HCl(V-1, J) + Cl_2$ (R-5)

b. $HCl(V, J) + Br \rightleftarrows HCl(V-1, J) + Br$ (R-6)

c. $HCl(V, J) + Cl \rightleftarrows HCl(V', J') + Cl$ (R-7)

3. R–R,T

$HCl(V, J) + M \rightleftarrows HCl(V, J') + M$ (R-8)

$M = Cl_2, Cl, HBr, HCl, Br$ (buffer gas)

of these photons due to output coupling and dissipative processes (e.g., diffraction). The explicit expressions for the various terms in eqs. (1,2) and the equations for the translational temperature and the non-lasing species are described below. A total of 70 vib-rotational levels are included in the simulation. The levels considered are $J = 0 - 25$ in the $V = 0$ manifold, $J = 0 - 20$ in $V = 1$, $J = 0 - 16$ in $V = 2$ and $J = 0 - 9$ in $V = 3$. $V = 0,1,2$ are pumped by the chemical reaction Cl + HBr → HCl + Br while $V = 3$ may be populated by energy transfer processes. Radiative transitions (primarily P-branch) are considered only for the $V = 2 \rightarrow 1$ and $V = 1 \rightarrow 0$ bands.

2.1. Radiation

The radiative terms $R(V, J)$ and $G(\nu)$ in eqs. (1,2) involve contributions from stimulated and spontaneous emission. For the pressure and temperature range considered in this work ($P \approx 1 - 10$ torr, $T \approx 300 - 600$ K) the spectral lines are mainly Doppler broadened [2]. $\Delta\nu_D \approx 10^{-2}$ cm^{-1} is about an order of magnitude larger than the homogeneous line width. For a laser cavity $L = 60$ cm long [2] the separation between the longitudinal modes $\Delta\nu = 1/2L \approx 10^{-2}$ cm$^{-1} \approx \Delta\nu_D$, i.e., there is (about) one cavity mode for each spectral line. We assume that one mode corresponds to the line center of the Doppler profile and that translational relaxation restores immediately the gaussin lineshape so that hole burning effects can be ignored.

There are four transitions associated with each V,J level; two P-branch transitions $V+1, J-1 \rightarrow V, J$ and $V, J \rightarrow V-1, J+1$ and two R-branch transitions $V+1, J+1 \rightarrow V, J$ and $V, J \rightarrow V-1, J-1$. As in the case of rotational equilibrium [8,16] we found that the R-branch transitions are weak and could be ignored.

Using $\rho_{V,J}$ to denote the photon density in the $P_{V \rightarrow V-1}(J)$- transition $V, J-1 \rightarrow V-1, J$ the gain term $G(\nu) \equiv G(V, J)$ in eq. (2) reads

$$G(V, J) = \alpha_{V,J}\rho_{V,J} + A'_{V,J}N_{V,J-1}. \qquad (3)$$

$A'_{V,J}$ is proportional to the Einstein coefficient $A_{V,J}$ ($A'_{V,J} \ll A_{V,J}$) and represents the effective number of spontaneously emitted photons with frequency corresponding to the oscillating mode. The gain coefficient at the line center of the Doppler line $\alpha_{V,J}$ is given in table 2.

Table 2
Spectroscopic data, rate constants and initial conditions [a,b]

(I) *Radiation* (P-branch, $h\nu_{V,J} = E_{V,J-1} - E_{V-1,J}$):

$$\alpha_{V,J} = c\sigma_{V,J}\{N_{V,J-1} - [(2J-1)/(2J+1)]N_{V-1,J}\} = c\sigma_{V,J}\Delta N_{V,J}$$

$$\sigma_{V,J} = \left(\frac{4\ln 2}{\pi}\right)^{1/2} \frac{A_{V,J}\lambda^3_{V,J}}{8\pi c}\left(\frac{\nu_{V,J}}{\Delta\nu_D}\right) = \frac{\lambda^3_{V,J}}{8\pi^{3/2}}\left(\frac{m}{2kT}\right)^{1/2} A_{V,J}$$

$$A_{V,J} = A_{V,J-1\to V-1,J} = A^V_{V-1}(\nu_{V,J}/\nu_{01})^3 J F_J/(2J-1) \text{ [17]}$$

$$F_J = 1 + 8(B_e/\omega_e)J = 1 + 0.03J \text{ [18]}, \quad A^1_0 = 34.6\ s^{-1}, \quad A^2_1 = 59.4\ s^{-1} \text{ [19]}$$

$$\alpha_{V,J} = 2.62 \times 10^{-5} a_V \left(\frac{J}{2J-1}\right) F_J \left(\frac{300}{T}\right)^{1/2} \Delta N_{V,J}, \quad a_1 = 1, \quad a_2 = 1.88$$

$$\Delta\nu_D(300\text{ K}) \approx 7 \times 10^{-3}\ \text{cm}^{-1}, \quad \rho_0 = 10^2\ \text{photon/cm}^3, \quad \tau_p = 4 \times 10^{-8}\ \text{s}, \quad \Delta N_{th} = (c\sigma_{V,J}\tau_p)^{-1} \approx 10^{12}\ \text{molec/cm}^3$$

(II) *Initiation*:

$$Cl_2 \xrightarrow{\text{flash}} 2Cl \qquad \text{(R-1)}$$

$$-d[Cl_2]/dt = F(t)[Cl_2]$$

$F(t) = K(t^2 + \alpha t)\exp(-\gamma t)$ (fig. 2)

$K = 2.5 \times 10^{13}\ s^{-3}, \quad \gamma = 4 \times 10^4\ s^{-1}, \quad \alpha = 8 \times 10^{-6}$ s

$[Cl_2]_0 = 2 \times 10^{17}$ molec/cm^3, $\quad [HBr]_0 = 5.8 \times 10^{16}$ molec/cm^3

(III) *Pumping*: $Cl + HBr \rightleftarrows HCl(V,J) + Br$ (R-2)

$$-d[HBr]/dt = d[HCl]/dt = k[Cl][HBr]$$

$$k = \sum_{V,J} k(\to V,J); \quad k(\to V,J) = kp(V)\,p(J|V); \quad \sum_V p(V) = \sum_J p(J|V) = 1$$

$k = 7.6 \times 10^{-12}$ cm^3/molec s [22]. $\quad p(V=0):p(1):p(2) = 0.3:1.0:0.4$ [20]

$p(J|V)$ – fig. 1

(IV) *Energy transfer*:

1. $V-V$

a. $HCl(V,J) + HCl(m,L) \rightleftarrows HCl(V \pm 1,J') + HCl(m \mp 1,L')$ (R-3)

$\Delta E = |E_{V,J,m,L} - E_{V\pm1,J',m\mp1,J,L'}| \leqslant 30\ \text{cm}^{-1}, \quad |J-J'|, |L-L'| \leqslant 2$

Given V,m, all transitions consistent with ΔE, ΔJ, ΔL equally probable

$$k(V,V' \to m,m') = \sum_{J,L} P(J)P(L) \sum_{J',L'} k(V,J,m,L \to V',J',m',L')$$

$P(J)$, $P(L)$ = Boltzmann rotational distributions

$k(2,0 \to 1,1) = 5 \times 10^{-12}$ [25–27]; $\quad k(3,0 \to 2,1) = 1.28\,k(2,0 \to 1,1) = 6.4 \times 10^{-12}$ [27];

$k(3,1 \to 2,2) = 15 \times 10^{-12}$ [$= 3k(2,0 \to 1,1)$, 'harmonic oscillator behavior']

b. $HCl(V,J) + HBr(0,L) \rightleftarrows HCl(V-1,J') + HBr(1,L')$ (R-4)

$\Delta E \leqslant 30\ \text{cm}^{-1}, \quad \Delta L, \Delta J \leqslant 2$

$k(V \to V-1) = Vk(1 \to 0) = V \cdot 1.1 \times 10^{-12}$ [31]

Table 2 (continued)

2. $V-R,T$ *transfer*

a. $HCl(V,J) + Cl_2 \rightleftarrows HCl(V-1,J') + Cl_2$ (R-5)

$k(V \to V-1) = Vk(1 \to 0) = V \cdot 5 \times 10^{-15}$ [33]

b. $HCl(V,J) + Br \rightleftarrows HCl(V-1,J) + Br$ (R-6)

$k(1 \to 0) = 3 \times 10^{-13}$, $k(2 \to 1) = 1.5 \times 10^{-12}$ [34]

c. $HCl(V,J) + Cl \rightleftarrows HCl(V',J') + Cl$ (R-7)

For $V' < V$, J' given by $E_{J'} = E_J + 0.7\Delta E_V$

$k(V,J \to V',J') = k(V \to V') + a(J-b)$; $a = 1.4 \times 10^{-12}$, $b = 3.0$

$k(1 \to 0) = 7.5 \times 10^{-12}$, $k(2 \to 1) = 9 \times 10^{-12}$, $k(2 \to 0) = 3.5 \times 10^{-12}$

$k(3 \to 2) = 9.7 \times 10^{-12}$, $k(3 \to 1) = 5 \times 10^{-12}$, $k(3 \to 0) = 2.2 \times 10^{-12}$

3. $R-R,T$ *transfer*

$HCl(V,J) + M \rightleftarrows HCl(V,J') + M$ (R-8)

$k(J \to J' < J) = W(2J'+1)\exp[-C(E_J - E_{J'})]$, $\Delta J \leqslant 2$

$k(J' \to J > J') = W(2J+1)\exp[-(C + 1/kT)(E_J - E_{J'})]$

Reference, $(Q/\Sigma_{J'}k(8 \to J') = 10$, $T = 300$ K), $W = 4.5 \times 10^{-12}$, $C = 0.007$ cm

a) All rate constants in units of cm^3/molec s.

b) All reversed rate constants calculated by detailed balance at the appropriate (time dependent) temperature.

The ratio between the induced and spontaneous emission terms in eq. (3) is of the order of the photon number density. Thus, during the lasing the second term in eq. (3) is negligibly small: yet, a finite amount, however small, of spontaneously emitted photons is essential for starting the amplification process. For reasons of numerical convenience we ignore the spontaneous emission term in eq. (3) and instead let the photon density develop from some low (noise) level of photons ρ_0 (table 2) when threshold is attained. Due to the very steep rise in the photon density after threshold the choice of the noise level hardly affects the laser output pattern.

The term $L(\nu) = L(V,J)$ incorporates all output and other losses of photons from the laser cavity. Assuming that τ_p, the average lifetime of photons in the cavity, is independent of the frequency we have $L(V,J) = \rho_{V,J}/\tau_p$. In a first approximation the output coupling of laser radiation can be taken as a constant fraction k, of the total loss $L_c = kL$. (Airey's estimate is $k \approx 0.2$ [2]). The value of k determines the magnitude of the pulse energy but does not influence the spectral distribution of the laser output. All calculations were carried out using $\tau_p = 4 \times 10^{-8}$ s corresponding to a total loss of about 10% per roundtrip.

The photon density $\rho_{V,J}$ in $P_{V \to V-1}(J)$ is thus given by

$$d\rho_{V,J}/dt = (\alpha_{V,J} - 1/\tau_p)\rho_{V,J}. \quad (4)$$

The radiation term $R(V,J)$ representing the influence of stimulated emission on $N_{V,J}$, eq. (1), is given by

$$R(V,J) = \alpha_{V,J+1}\rho_{V,J+1} - \alpha_{V+1,J}\rho_{V+1,J}. \quad (5)$$

In fact, eq. (6) applies only to $V = 1$; for $V = 0$ the first term is missing while for $V = 2$, since there is no lasing from $V = 3$, the second term is practically zero. When R-branch transitions were taken into account the corresponding terms were added to eq. (6). Spontaneous emission terms, being of negligible importance, have not been included in eq. (1).

2.2. Pumping

Neglecting the reversed processes of (R-2) (see below) the pumping term in eq. (1) is

$$P(V,J) = k(\to V,J)[Cl]\,[HBr], \quad (6)$$

where $k(\to V,J)$ is the rate constant from thermal reactants to $HCl(V,J)$ products, fig. 1. The Cl atoms are produced by flash photolysis, tables 1,2 and fig. 2, with

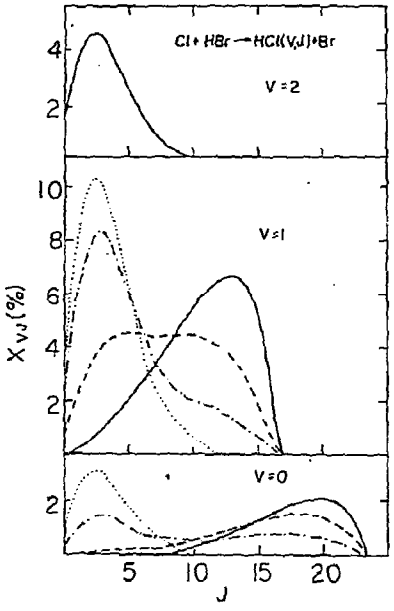

Fig. 1. Rotational distribution functions of HCl(V) (in % of population) for pre-threshold times obtained from simulation with $Z_{rot} = 0.2$ (high $R - T$).

Solid line: nascent product distribution of the reaction ($t = 0$); (----): after 130 collisions ($t = 0.05$ μs); (-·-·-): after 520 collisions ($t = 0.2$ μs); (. . . .): after 2500 collisions ($t = 1$ μs).

a flash profile $F(t)$, fitted to that in ref. [2]. The 'hot' Cl atmos produced in (R-1) are assumed to cool down instantaneously. The initial vib-rotational distribution $p(V, J)$ is based on chemiluminescence data [20,21], the absolute values were scaled from $\Sigma_J k(V, J)$, ref. [22]. The reported values of $P(V = 0)/P(V = 1)$ is 0 – 0.6; the value 0.3 fits best the experimental pulse duration [2]. The nascent rotational distributions shown in fig. 1 are based on the maxima reported in [21] and the assumption that their shape is similar to rotational distributions in other halogen–hydrogen halide reactions [21]. Because of the exothermicity of (R-2) the reversed reaction is negligibly slow, except for high V, J levels [23]. Therefore only transitions from $V = 3$ were taken into account.

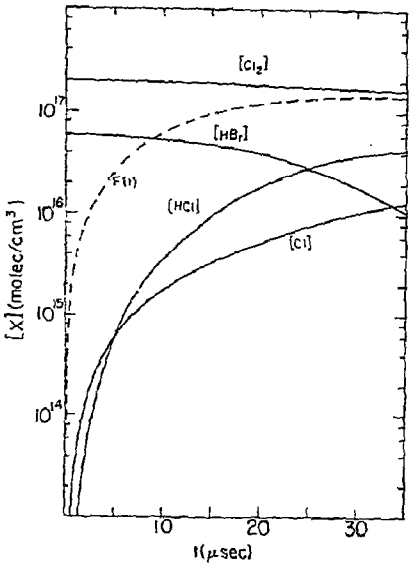

Fig. 2. Time-variation of the concentrations X of the molecular species (independent of Z_{rot}).

2.3. Energy transfer processes

2.3.1. $V - V$ transfer

(a) HCl – HCl – As a typical example for the contribution of relaxation processes to $D(V, J)$ in eq. (1) consider the influence of $V - V$ exchange in HCl–HCl collisions, (R-3). Using obvious notations this contribution is

$$V\text{–}V_{HCl}(V,J) = \sum_{m,L,V',J',m',L'} [k(V,J,m,L \to V',J',m',L') \times N(V,J)N(m,L) - k(V',J',m',L' \to V,J,m,L)N(V',J')N(m',L')] \quad (7)$$

Since multi-vibrational quanta exchange is improbable [24] we only consider $V' = V \pm 1$, $m' = m \pm 1$. Thermal (averaged over J, L) rate constants were measured [25–28] but there is no information on their J dependence. Based on the dipole–multipole theory of Sharma and Brau (SB) [29] it was assumed that all transitions with $\Delta E \leqslant 30$ cm^{-1} occur with the same rate. Transitions corresponding to higher energy mismatch are disregarded. The $\Delta J \leqslant 2$ rule follows from the first order

perturbation approximation [29]. (See however [30].) After counting all the allowed J, L, J', L' combinations the rate constants are normalized to yield the experimental thermal values. Resonant transitions, $V, V+1 \rightarrow V+1, V$, are efficient [26] and may cause small local irregularities in the nonequilibrium rotational populations. Nevertheless, we ignore them since the fast R–T processes will smooth over these effects. All V–V rate constants are assumed to vary according to T^{-1} [28,29].

(b) HCl–HBr – Reaction (R-4) is near resonant with $\Delta E \approx 100 - 300$ cm^{-1} and therefore not significantly slower than (R-3). The HBr molcules are assumed to be in thermal equilibrium. Hence, due to the large excess of HBr(0) molecules (R-4) provides the main vibrational relaxation route. For further details see table 2.

2.3.2. V – R, T energy transfer

Vibrational relaxation accompanied by V–R transfer may lead to changes in the rotational distributions of the lasing molecules. The fine details of the rota tional structures arising from V–R transfer are largerly erased by the generally much faster R–R,T and V–V processes. In view of this fact the lack of detailed information about the initial and final J dependence of the V–R,T rate constants is not a serious limitation since only their gross features are expected to be reflected in the spectral distribution of the laser output.

V→R transfer seem to be the main deactivation mechanism in HCl–HCl and HCl–HBr collisions [31, 32]. The rates of V–R,T transfer in these collisions are, however, negligible compared to the corresponding V–V rates and we do not include therm in the kinetic model. (Note that (R-3) is effectively a V–T process so neglecting HCl–HBr V–R,T transfer is completely justified. HCl–HCl collisions are anyhow quite rare.)

(a) HCl–Cl$_2$ – (R-5) is a slow process [33] but may be effective because of the large Cl_2 concentration. A pure V–T, ($J' = J$), and harmonic V-dependence of the rate constants were assumed.

(b) HCl–Br – In view of the low value of [Br], fig. 2, and the moderate rate constants of (R-6) [33,34] HCl–Br collisions cannot significantly affect the HCl(V, J) populations. Thus, although V–R transfer is probably the main mechanism here [35,36] we assumed $J' = J$.

(c) HCl–Cl – The thermal rate constant of the $V = 1 \rightarrow 0$ transition in (R-7) is reported in refs. [22,37] (see also [40]). Classical trajectory studies [36,38,39] indicate that: (1) The rates increase with J. (2) V→R is the major deactivation mechanism. (3) $\Delta V > 1$ jumps are probable. (4) $k(V \rightarrow V-1) \neq Vk(1 \rightarrow 0)$. (5) Reactive collisions. (The exact J dependence and the relative efficiency of V→R and V–T were not reported.) Based on this partial information it was assumed that $2/3\Delta E_v$ is released as HCl rotational energy (V→R/V→T = 2). Furthermore, it was assumed, mainly for computational convenience, that the gain in rotational energy is concentrated in one final J' level. Small irregularities which could arise from this 'selection rule' are largely masked by the fast R–R,T and V–V processes. A linear J dependence, similar to that found for Br + HBr [35], was adopted. Further details are provided in table 2.

2.3.3. R–R,T transfer

The rotational transition probabilities corresponding to (R-8) are based on Ding and Polanyi's modification [41] to the Polanyi and Woodall model [21]. In view of the high sensitivity of the laser output to the rate of rotational relaxation and the lack of accurate information on absolute R–R,T rates we have treated W, table 2, as a free parameter measuring the efficiency of R–T transfer. The reference value of W corresponds, for $k(J \rightarrow J')$, to one transition every ten collisions for $J = 8$ [where $k(J \rightarrow J = 1)$ reaches its maximum]. The common estimate for the rotational collision number is: $Z_{rot} = Q/\Sigma_{J'} k(J \rightarrow J') = 10$ [42] where Q is the hard sphere collision frequency. The temperature dependence of $k(J \rightarrow J')$ was taken only through the collision frequency, $Q \propto T^{1/2}$.

Finally, if the absolute value of the rotational transition probabilities were known, increasing W is approximately equivalent to adding a buffer gas to the laser system to selectively enhance rotational relaxation. We have exploited this analogy and studied the effect of rotational relaxation rate on the laser performance by varying W over a wide range corresponding formally, to $Z_{rot} = 0.2$–33. The analogy should not be taken as fully quantitative since other pressure dependent fac-

tors such as the line broadening mechanism and the equation governing the translational temperature rise were not changed (but kept as for the reference choice of W). (Only at the highest value of W corresponding to $Z_{rot} = 0.2$ pressure broadening becomes comparable to $\Delta\nu_D$. See also section 4.)

2.4. Translational temperature

The translational temperature enters the rate equations as a parameter influencing the various rate constants (including those for stimulating emission via $\Delta\nu_D$, eqs. (4), (5)). The main contributions to the rise in the heat bath temperature comes from the residual flash energy (the excess flash energy over the dissociation energy of Cl_2) and the translational exothermicity of the pumping reaction [2]. We ignore the contribution of V → T transfer and add the R → T contribution to the translational exothermicity (this approximation becomes exact in the limit of very fast rotational relaxation). Thus, following Airey [2] the temperature equation is

$$dT/dt = n F(t)[Cl_2] + mk[HBr][Cl]. \quad (8)$$

where $m = 8 \times 10^{-15}$ cm^3 deg/molec corresponds to the fraction $(2/3)$ of the pumping reaction energy going into translational + rotational degrees of freedom. $n = 1.1 \times 10^{-14}$ cm^3 deg/molec corresponds to the fraction (14.3 kcal/mole) of the flash energy.

3. Numerical method

The coupled non-linear rate equations involve fastly changing variables. They present severe stability problems and can be classified as stiff equations [43]. The fundamental numerical tool employed in the calculations is a modification (allowing for variable dimensionality) to Brumer's version [45] of Gear's hybrid (predictor–corrector integrator) method [44]. All calculations were carried out on the IBM 370/165 of the Weizmann Institute of Science.

4. Results and analysis of the simulations

In describing the calculations we carried out and the conclusions we drew, it is profitable to use as a convenient frame of reference Airey's [2] picture of the Cl + HBr laser. While this important pioneering model is (as we shall see) in many respects rather remote from the real physical situation, it is nevertheless advantageous to outline our results as a series of quantitative tests of the deviations from a computationally and conceptually simple framework. Three basic assumptions can be said to define Airey's model:

(i) *Steady-state operation*: It is supposed that the photon density satisfies a steady-state condition, this being in fact the lasing threshold equation. Given that the populations of the states involved in radiation are determined at any time from the rate equations, the photon density can then be obtained from the (algebraic) threshold condition.

(ii) *Single line operation*: Lasing is assumed to take place on a single rotational line only at any given instant, the line with the highest gain.

(iii) *Rotational equilibrium*: The rotational states are taken to be in equilibrium, at any given time, their temperature being the translational one. After any pumping or radiation event the rotational distribution function is, supposedly, instantly restored to equilibrium by R–T processes.

While all the above assumptions will be quantitatively examined below, the "rotational equilibrium postulate" is clearly the most important and essential of these, so the investigation of this aspect will be at the center of the present article.

4.1. Test of the steady-state, on-threshold operation assumption

To test this approximation, the kinetic equations of the laser were solved in the framework of the single line model and the rotational equilibrium assumption, but the steady-state treatment of the photon density was removed. Instead the photon density was evaluated from the appropriate differential rate equation, coupled with the equations for the populations of the states involved in the radiative process. The results of the calculation, together with those obtained from Airey's model [2] and from the experimental work of this author [2] are shown in fig. 3. In comparing the calculations with the experimental result one must keep in mind the relatively poor time-resolving power of the apparatus [2]. In particular, narrow threshold peaks were not observable in this experiment. The pulse-shape

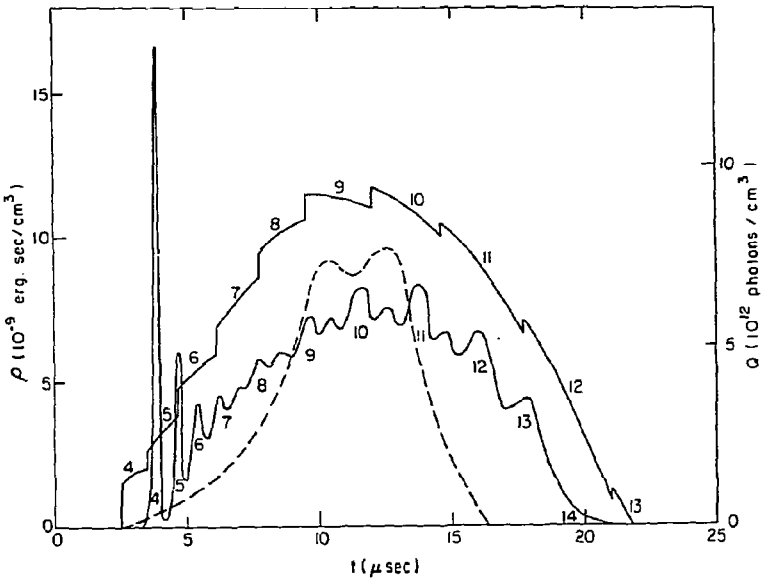

Fig. 3. Time-dependence of the laser pulse. (-----): Airey's experiment [2]. Jigsaw solid line: Airey's steady-state, (on-threshold) approximation. Smooth-solid line: single line, rotational equilibrium model (rate equation used to calculate the photon density ρ). Numbers indicate the radiating J-level.

given by calculations should perhaps be "coarse grained" somewhat to correspond to the experimental result. In these terms it is clear that the results of our calculation, based on assumptions (ii) and (iii) only, fits the experiment better than Airey's. The steady-state approximation is seen (fig. 3) to give a too high total output intensity. Also, elimination of the steady-state approximation led to disappearance of the unphysical jigsaw-structure of ref. [2]. The jigsaw pattern is an artifact of the way in which the photon density is computed in the framework of assumption (i) above, by keeping the inversion density at the threshold value. This gives an algebraic equation for $\rho_{V,J}(=\rho_{\text{tot}})$ that varies continuously with time so long as radiation is supposed to take place from the same transition. When the maximum gain condition predicts a new J-transition the entire photon density is attributed to the latter, and the algebraic expression will yield in general a jump in the value of the photon density ρ_{tot} as one goes from $\rho_{V,J}$ to $\rho_{V,J'}$. The differential equation approach enables one to maintain continuity. Another important, although obvious, point to note in fig. 3 is that deletion of the steady-state approximation produces the threshold relaxation oscillations.

It is of special interest, however, that the stationary-state treatment does seem able to predict adequately some nontrivial effects. This may suggest its use in a limited way in future approximation schemes. We note from fig. 3 that *Airey's model predicts the shift to higher J-transitions in the pulse in good quantitative agreement with the more complicated calculation.*

Since the subject will prove of significance also in further developments, we shall briefly discuss it below. We assume first only the postulate of rotational equilibrium, but not the approximations (i) or (ii). A necessary condition for radiation on a P-branch is [16,17]:

$$N_{V,J-1} - [(2J-1)/(2J+1)]\,N_{V-1,J} > 0, \qquad (9)$$

where $N_{V,J}$ is the population of the (V,J)th vib-rotational species. Using the rotational equilibrium postulate we have:

$$(X_V/Q_V)\exp[-B_V J(J-1)/kT] - (X_{V-1}/Q_{V-1})\exp[-B_{V-1}J(J+1)/kT] > 0. \qquad (10)$$

Q_V and B_V denote respectively the rotational partition function and the rotational constant at the vibrational

level V. Assuming now the rigid rotor approximation, in which framework B_V and Q_V are V-independent, we get from (10) that radiation can take place only from J-values such that:

$$J \geqslant J^* \gtrsim (kT/2B) \ln(X_V/X_{V-1}), \tag{11}$$

where J^* is the *smallest* integer for which inequality (11) holds. With the exception of the few lowest J's, J^* corresponds to the highest gain transition. To confirm this write $\alpha_{V,J} = C[\sigma_{V,J}/(2J-1)]\,[(2J-1)\Delta N_{V,J}]$, (cf. table 2). As $\sigma_{V,J} \propto J$ the main J dependence of $\alpha_{V,J}$ is in the exponential terms in $(2J-1)\Delta N_{V,J}$. The maximum gain condition becomes

$$\mathrm{d}\alpha_{V,J}/\mathrm{d}J \approx \mathrm{d}(2J-1)\Delta N_{V,J}/\mathrm{d}J = 0, \tag{12}$$

or, explicitly

$$J\,(\text{max. gain}) \approx \frac{kT}{2B} \ln\left(\frac{X_V}{X_{V-1}}\,\frac{2J-1}{2J+1}\right) \approx J^*. \tag{13}$$

Expression (13) predicts a shift to higher-J transitions with increasing time as a result of two factors:

(1) An increase in the translational temperature as a result of heating.

(2) A decrease in the "vibrational temperature", i.e., in the ratio X_V/X_{V-1} with time. As a consequence lasing will be due to progressively larger J. Quantitatively, our calculation based on postulates (ii) and (iii) indicated that, in the present system, (2) is the dominant effect in causing funneling, and the effect of translational heating is small except towards the end of the pulse. We shall see that a substantial part of the above conclusions can be retained also for the results of the "full" simulation. Similar conclusions were reached in the simulation of ref. [14] on the HF laser.

So far we discussed the funneling effect in the framework based on assumptions (ii) and (iii) only. In the steady-state model, the photon-density is computed by imposing the laser-threshold condition on the highest gain transition [2].

$$\alpha_{V,J} = C\sigma_{V,J}\Delta N_{V,J} = 1/\tau_p = \text{const.} \tag{14}$$

To sum up, from the calculations we carried out and the simple theoretical considerations above, one can draw the following conclusion: The Airey model, based on assumptions (i)–(iii) yields the correct time-dependence of the lasing frequency and the rough envelope of the laser pulse-shape. However, the steady-state approximation, even when (ii) and (iii) are valid, leads to an incorrect detailed structure of the pulse (nonphysical jumps, absence of threshold oscillations) and to too large magnitudes of the output intensity.

4.2. The single line assumption

The validity of this assumption was examined first when the more fundamental rotational equilibrium postulate was taken to hold. Thus the laser kinetic equations were solved in the framework of postulate (iii), but multiline laser operation was allowed for by including the rate equations for all the possible active photon densities, suitably coupled with the equations for the populations. The results are presented in fig. 4. The main conclusion is that *when rotational equilibrium holds, the assumption of single line operation constitutes an extremely good description of the actual situation.* Unlike in the calculation of section 4.1 above, each line obviously begins from the noise level rather than from the value of the radiation density of the previous line at the instant of changeover. This leads to some overlap of lines at the tails of individual J-pulses, but the effect is very small indeed and the peaks are basically well-resolved. The same conclusion has been reached also in refs. [13,14], and is intuitively not surprising: The instantaneous rotational relaxation prevents any hole-burning in the rotational distributions pertaining to both the upper and the lower vibrational states. Radiation begins on some J-transition, and the mechanism described in section 4.1 explains the shift to higher J's with time. But given that no holes are burnt in the rotational distribution functions and that these retain the Boltzmann shape, there seems no reason to expect that a high gain situation will develop simultaneously for some additional, further J. In fact the numerical results we obtained show more precisely that the negligible extent of the overlap is caused by the instantaneous draining of inversion density towards the highest gain line as a consequence of the infinitely fast R–T relaxation. As evident from the discussion in section 4.1 a new level J cannot begin to lase before J^* (defined in (11)) is greater than $J-1$. When this happens the gain from the previous $J-1$ line becomes negative and the latter decays quickly. Our calculations show also that instantaneous R–T leads to pronounced relaxation oscillations at the beginning of every J-pulse. The first peak is the highest since it occurs when the inversion is greatest, in fact when the

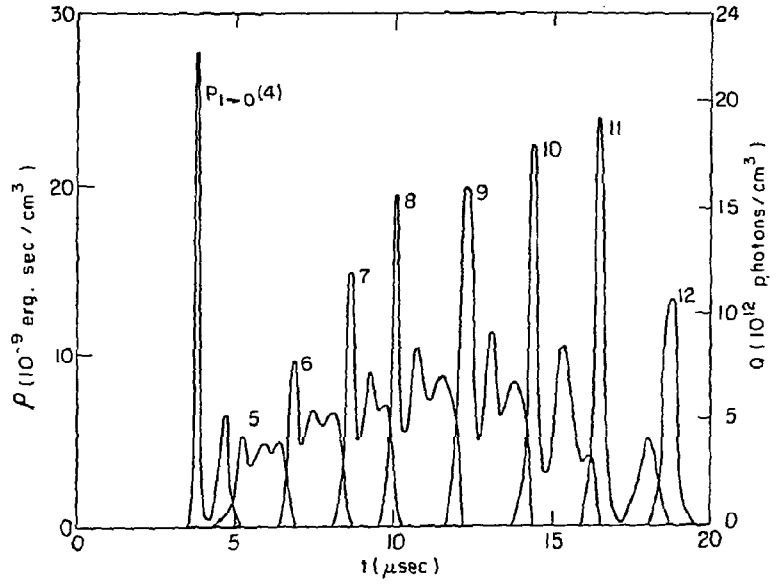

Fig. 4. Radiation densities of individual J-pulses, instantaneous R–T, multiline operation. Right-hand scale is in units of photon density, left-hand scale in units of radiation density.

system is *totally inverted*. As it turns out, all the subsequent peaks correspond to partially inverted transitions.

We found that single line operation follows almost directly as a consequence of rotational equilibrium. In the forthcoming part of the study we shall see that in the absence of this condition the single line model breaks down completely.

4.3. Test of the rotational equilibrium postulate, and the nature of rotational nonequilibrium effects

From sections 4.1 and 4.2 above it is clear that the question whether rotational equilibrium holds is of critical importance for the direct prediction of many aspects of laser action, not to mention its significance in reducing the numerical labour involved in solving the rate equations. Most of the effort of the present article is thus directed towards this question. To study it in detail a number of computer simulations of the laser system were carried out, each at conditions representing different average rotational relaxation (R–T) rates. In this way the existence of rotational nonequilibrium effects could be examined over the entire range of rotational relaxation rates consistent with experimentally feasible conditions. The set of simulations were thus carried out for $Z_{rot} = 33,20,10,5,2.5,1,0.2$, where Z_{rot} is the ratio between the gas kinetic cross section and the corresponding average rotational relaxation cross section for an HCl molecule in the system. Given the molecular constitution of the laser in Airey's experiment, the correct value is around $Z_{rot} \approx 10$. It may at first appear nonphysical to consider $Z_{rot} < 1$ values since for all molecules the rotational relaxation cross section is smaller than the elastic (gas kinetic) one. Nevertheless, the consideration of such Z_{rot} values is not purely formal but can be given a physical interpretation: Suppose that we are adding an inert gas to the laser system and that the only effect of this gas is to cause rotational relaxation of the HCl molecules. (This is not an unreasonable assumption, at least as a first approximation since the other relaxation effects due to the inert gas, such as a V–T, are of much less importance in influencing the effects under investigation here.) The effect of the inert gas on the laser can then be modelled by increasing Z_{rot} in the rate equations, an increase that is linear in the pressure of the added gas. In each simulation, all the relevant vib-rotational populations and photon densities were treated as independent, unknown functions and obtained by

solving the master equations. In the equations all pumping, radiation, relaxation and energy transfer processes were included with realistic rate constants. (For the details of all this see section 2.) The only exception was the V–V process for HCl–HCl collisions: This effect was included fully (including the dependence of this transition on the rotational states of the molecules) in the run with $Z_{rot} = 10$. It was found to have negligible importance on all aspects of interest, so only the average (over the J-states) of this process was included in the simulations with other Z_{rot}. Full inclusion of the V–V process is numerically time consuming since it leads to many terms in the rate equations.

4.3.1. Strongly overlapping rotational lines – evidence for rotational nonequilibrium effects

We begin our discussion of the results of these "computer experiments" with fig. 5, showing the pulses for all individual J values ($J = 1–16$) of the P-branch vibrational transition in the cases $Z_{rot} = 33,10,2.5,0.2$. (Enlarged drawing of two representative J lines are given in figs. 6 and 7). The main striking feature of the result is that in all these cases, including $Z_{rot} = 0.2$ (very high R–T) is there substantial overlap between different J-lines. We saw already in section 4.2 that rotational equilibrium is a sufficient condition for single line operation. We conclude that *even when the R–T rate is much higher than in Airey's experiment* (due, say, to high pressure of an added inert gas) the *rotational equilibrium assumption is not valid for the laser under consideration.* As the rate of rotational relaxation is decreased, the individual J-pulses shown in fig. 5 become lower, wider and overlap more extensively. As

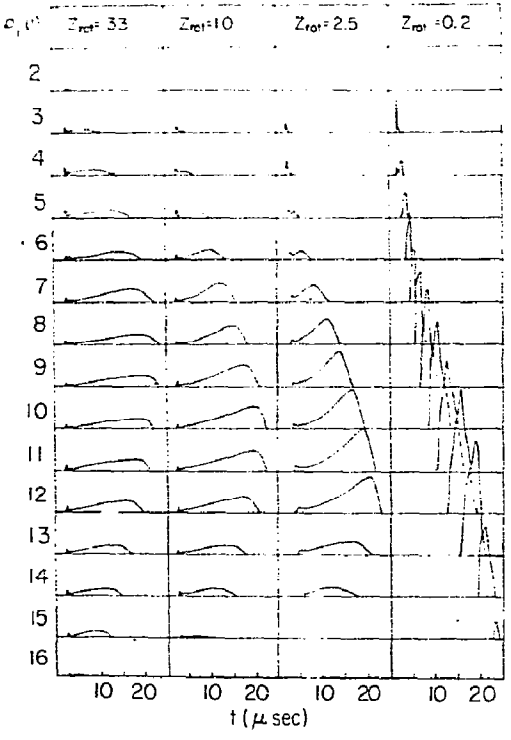

Fig. 5. Photon densities of individual J-lines as function of time (for 4 values of the R–T rate). J-number is indicated on the left side. P.D. scale – 4.5×10^{12} photons/cc. Time scale – 25 μs.

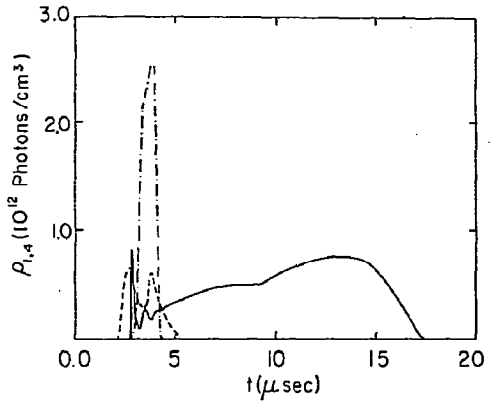

Fig. 6. Photon density of $P(V = 1, J = 5)$ line as functions of time [for $Z_{rot} = 0.2$ (dash-dotted line), 2.5 (dashed line), 3.3 (solid line)].

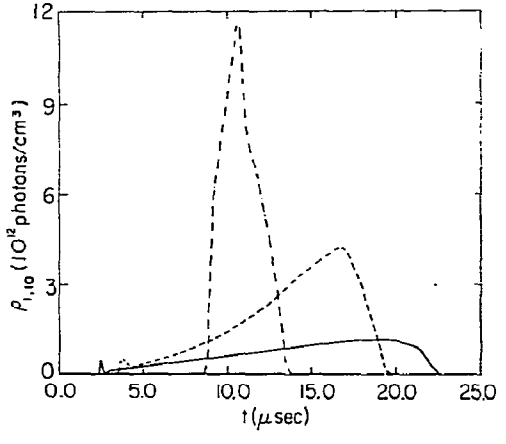

Fig. 7. Photon density of $P(V = 1, J = 10)$ line as function of time (for $Z_{rot} = 0.2; 2.5; 33$; other notation as in fig. 6).

would be expected, the case $Z_{rot} = 0.2$ is the nearest to the rotational equilibrium picture, but even there two lines seem to lase simultaneously at any given time. With the other Z_{rot} values, many lines lase simultaneously over large intervals of the pulse. It is of considerable interest to express quantitatively the extent by which the case $Z_{rot} = 0.2$ differs from the ideal "rotational equilibrium" situation with regard to prediction of the intensity maxima. Fig. 8 compares the theoretical prediction of eq. (11), based on the rotational equilibrium model, with the actual positions of the peaks given by the computer simulation. The factors $kT(t)/2B$ and $\ln[X_1(t)/X_0(t)]$ both time-dependent were calculated from the simulation and plotted in fig. 8 (upper and lower curve, respectively). The value of $J^*(t)$ was then obtained by rounding off the product of these two factors to the nearest integer. The results, a sequence of horizontal lines is shown also on fig. 8 together with the correct positions of the peaks (each defined as the location of the maximum of the strongest J-pulse in the relevant time-interval). Good agreement is seen to exist between the values given by eq. (11) and the true positions of the peaks. We conclude that *for high R–T, eq. (11) offers a good approximation to the position of the pulse peaks despite the fact that neither the single line assumption nor the rotational equilibrium model hold in this case.* The result should be of considerable interest for approximate treatments of gas laser systems at high inert gas pressure. The same conclusion is not true

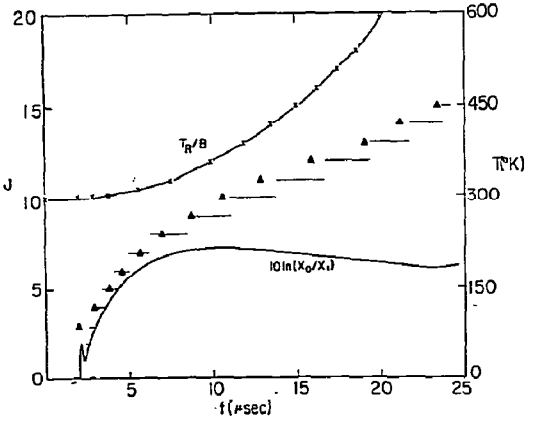

Fig. 8. J-shift of the highest peak with time ($Z_{rot} = 0.2$). Upper curve – calculated $T(t)/B$. Lower curve – calculated values of $10\ln(X_0/X_1)$. Horizontal lines – J^* calculated according to eq. (21). Triangles (▲) – J-number of the largest peak (from the simulation).

for lower R–T, including the "normal" value $Z_{rot} = 10$. The predictions of (11), the rotational equilibrium result, for $J > 10$ are (fig. 9) in poor agreement with the correct positions of the peak. Many lines then lase simultaneously, and there appears to be little correlation between the positions of the peaks and the maximum gain regions. In fact, many J-lines never reach a state of maximum gain: This is specially true for $J > 10$ (where also the J-shift of the peak with time appears to be negative). It is interesting to note, however, that the predictions of (11) for $J \leqslant 10$ in the normal case ($Z_{rot} = 10$, see fig. 9) are in good agreement with the correct peaks computed from the simulation. *Thus, even for moderate ("normal") R–T rates the rotational equilibrium estimate for the peak position has got predictive value, if restriction is made to sufficiently low values of J.* The reason is that for low J-values rotational relaxation is fast.

In the context of fig. 8 (for $Z_{rot} = 0.2$) a comment should be made on the relative importance of the translational temperature factor and the vibrational population factor (see eq. (11)) in causing the J-shift. Clearly if the translational temperature were constant, J^* in fig. 8 would have followed the time-dependence of the lower-solid curve, essentially the "vibrational temperature" curve. Similarly if X_0/X_1 were constant, the time-dependence of J^* would be that of the translational temperature. In the initial stages of the laser pulse the translational temperature is almost unchanged, and the behaviour of J^* is governed by $X_0(t)/X_1(t)$. After about 8 μs the curve $kT(t=0)/2B \ln[X_0(t)/X_1(t)]$ levels off around $J = 7$ and the translational heating of the system becomes responsible for the continuing J-shift (when rotational equilibrium prevails translational heating means also an increase in the rotational temperature).

4.3.2. The nonequilibrium rotational distribution functions

Using the phenomenon of overlapping lines as an indicator, we were able to show above that significant deviations from rotational equilibrium persist even for Z_{rot} as low as 0.2, and concluded that the model of rotational equilibrium must be a very poor representation of reality for the R–T rates of normal conditions in the laser system under consideration. We shall now examine this question more directly by looking at the forms of the rotational distriabution functions. Consider first the high R–T case, with $Z_{rot} = 0.2$. The pre-

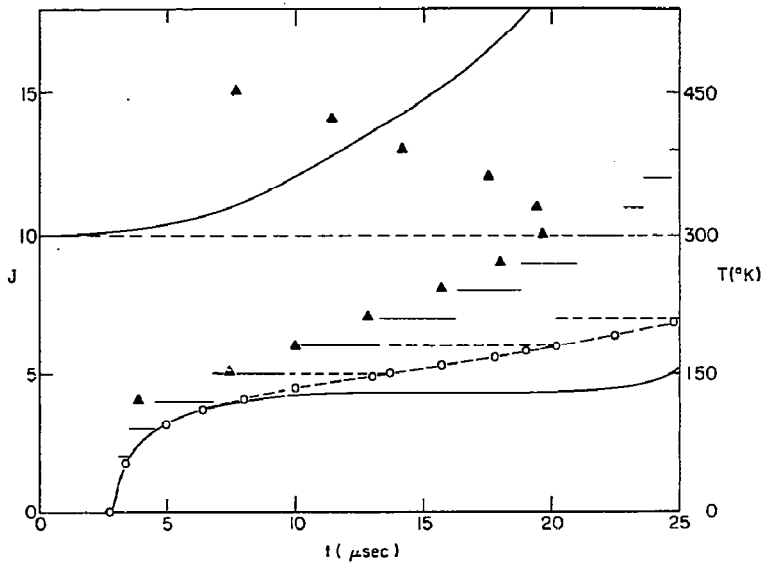

Fig. 9. J-Shift of the highest peak with time ($Z_{rot} = 10$) (with and without keeping the temperature constant). Solid upper curve – $T(t)/B$. Solid lower curve – $10 \ln(X_0(t)/X_1(t)$. Horizontal solid lines – J^* according to eq. (11), time-dependent of T included. Triangles – J-number of largest peak (simulation with varying temperature). Open circles – same as above for simulation with constant temperature. Horizontal broken line – J^* according to eq. (11) for run with constant T.

threshold time development of the distribution functions is shown in fig. 1. The nascent distribution functions are highly non-equilibrium ones, reflecting the nature of the pumping by the chemical reaction. R–T effects quickly build up, and the distribution function for both $V = 1$ and $V = 0$ assume after a few hundred collisions the double-hump Polanyi–Woodall form, typical of competition between R–T and pumping [21,48]. However, well before threshold, sharply peaked almost Boltzmann structures of the distribution function are obtained owing to the increasingly dominant R–T effects. The post-threshold situation, during laser action, is described in fig. 10. It becomes evident how the situation changes from total inversion at threshold to partial inversion around 2μs. *Throughout the entire development no holes are burnt in the upper rotational distribution structure by the laser action, and the nearly Boltzmann forms persist for both N(1,J) and N(0,J).* This explains quantitatively why in many respects laser action at $Z_{rot} = 0.2$ can be represented by the rotational equilibrium model. However, as we noted in section 4.1, significant, if relatively small deviations from the full equilibrium limit exist; *the maximum of the rotational distribution function is shifted towards higher J-values (when compared with the equilibrium case) as a consequence of the effects of pumping.* This is the reason why the correct values of the maximum peak in fig. 8 are higher than the values J^* predicted by the rotational equilibrium model. A much more drastic and qualitatively different deviation from the rotational equilibrium picture occurs in the "normal" R–T case, with $Z_{rot} = 10$. The rotational distribution functions at post-threshold times are shown for this case in fig. 11. *For both $V = 1$ and $V = 0$ the distribution functions are strongly non-Boltzmann with, essentially, a double-hump structure throughout the laser pulse.* At threshold times the rotational distribution function for $V = 1$ shows a Polanyi–Woodall structure with two very shallow maxima almost merging into a single broad peak. Unlike the case with $Z_{rot} = 0.2$, R–T does not dominate over pumping at the threshold time, so the competition between these two processes governs the structure of $N(1, J)$ at this stage. The distribution function for $V = 0$ has, at threshold, a single maximum located at $J = 17$. *During laser action both N(1,J) and N(0,J) develop and maintain double-hump structures* which are *not* due to the Polanyi–Woodall mechanism of pumping competing with rotational relaxation. Rather the double maximum

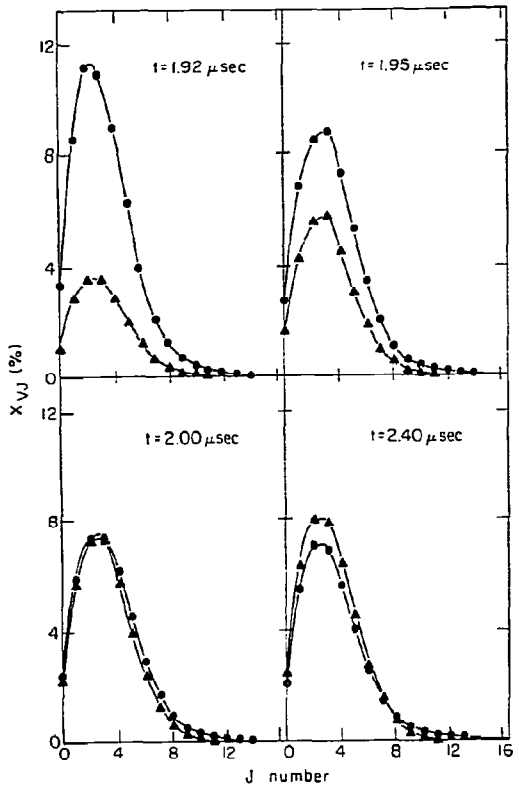

Fig. 10. Rotational distribution functions at post-threshold times (Z_{rot} = 0.2). (The triangles give the function for V = 0, the circles for V = 1.)

shape of $N(1,J)$ is due to population depletion at the lasing J's by the radiation. Similarly, the additional peak in the lower J's of $N(0,J)$ is built by the radiative cascades from the level V = 1. (The significance of hole burning effects in chemical lasers, in particular HF, has already been discussed by several authors [7,13,14].) Both the hole-burning effect in the V = 1 distribution function and the second peak building in the V = 0 distribution function are relatively "spiked" in the beginning of the laser pulse, but are partly smoothed by rotational relaxation in the later stages of the pulse. For low J-values, where rotational spacings are small and R–T cross section consequently large, the "smoothing" is faster than for the high J levels. This indeed, is also a major cause for the long persistance in time of the high-J maximum in $N(1,J)$. An inspection of fig. 12 suggests what we believe to be an important hint for future development of approximation techniques in the calculation of laser kinetics. It should be possible to represent $N(1,J)$ by a suitable guess function of simple analytic form having a double hump structure. A similar statement can be made for $N(0,J)$ except that at threshold only one maxima should be present. Should this be achieved, the many variables $N(V,J)$ could be replaced by simple analytic function of J, where the entire time dependence is carried by a few parameters that determine the double-hump function. The saving of computational effort should be very large.

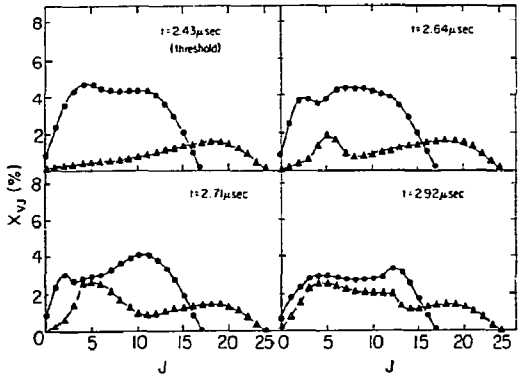

Fig. 11. Rotational distribution functions at post-threshold times (Z_{rot} = 10). (The triangles give the function for V = 0, the circles the function for V = 1.)

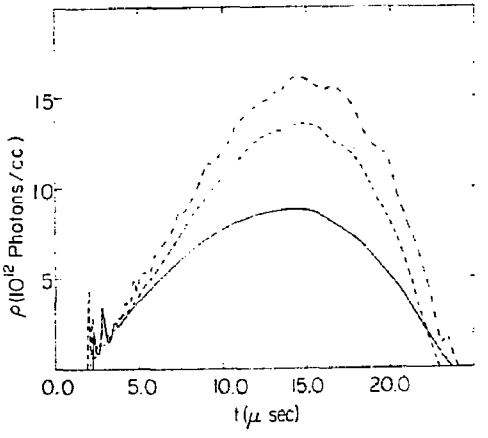

Fig. 12. Time-dependence of the total laser pulse intensity [for Z_{rot} = 33 (solid line), 2.5 (dashed), 0.2 (dash-dotted)].

4.3.3. Threshold oscillations and steady-state regions

We return to fig. 5 to examine the time-dependence of the photon densities for individual J-lines. For the "usual" R–T rate represented by $Z_{rot} = 10$ the behaviour is one of several rapid and receding oscillations following threshold, continued by a smooth and relatively slow rise to a (local) maximum at the late stage of the pulse, after which stage the intensity falls off quite steeply to the noise level as the pulse decays. The same pattern occurs also for almost all the other "R–T conditions" represented by the various Z_{rot} values employed. The following important trend can be observed in fig. 5: *For a given J value the higher Z_{rot}, the smaller is the oscillation region compared with the "slow" part of the pulse and the smoother becomes the later component.* The sharp oscillation peaks become, however, higher and narrower as R–T increases (i.e., Z_{rot} decreases). An exception to the trend mentioned are the high-J lines at $Z_{rot} = 0.2$ where no arrow threshold oscillations can be seen. The following interpretation can be given to the above mentioned trend. Near the rotational equilibrium limit ($Z_{rot} = 0.2$) the R–T effects dominate and lead to a draining of the entire inversion density into a single maximum gain line. The latter can greatly exceed the threshold density and lases far from the threshold steady-state conditions, giving rise to steep oscillations [49]. When the R–T rate decreases the pumping is no longer directed into a single level but distributed over several simultaneously lasing lines. The pumping rate for each transition is relatively weak to an extent that only near threshold operation is possible. Therefore the threshold oscillation will be moderate and an extended steady-state region will occur. Inspection of fig. 5 shows also that at a given Z_{rot}, an increased steady-state behaviour is obtained for J-levels for which the pumping is weak and R–T relaxation is slow. The interpretation is similar to that given for the previous trend. In general, a steady-state behaviour will threfore obtain for sufficiently large J's. This will be exploited in future models of laser kinetics [50].

4.3.4. Influence of R–T on total pulse and vibrational populations

The pronounced effects of rotational non-equilibrium discussed in the previous sub-sections were related to the behaviour of individual vib-rotational variables such as $N(V,J)$, the population of (V,J)th level, and $\rho(V,J)$, the photon density of a single P-branch line.

It is of interest to consider also the influence of rotational non-equilibrium on quantities integrated with respect to the J-states, such as the total radiation density and the (total) population of each vibrational level. The time-dependence of the total radiation pulse is shown in fig. 12 for $Z_{rot} = 33, 2.5, 0.2$. It is evident from this graph that the threshold time, the pulse duration, and the time-point of maximum output radiation are essentially independent of Z_{rot}, i.e., of the extent of rotational relaxation. The pulse shapes are, on the whole, very similar in all cases, if we keep in mind the very large change in Z_{rot} from one curve to another. The influence of Z_{rot} is considerable mainly in the relaxation oscillations at threshold. Fig. 12 is another manifestation of the observation made earlier that as we approach the rotational equilibrium limit, relaxation oscillations become more pronounced and extended. We also note from fig. 12 that the intensity maxima decrease moderately with Z_{rot}. Comparison of fig. 12 with the rotational equilibrium treatments, figs. 4, 3, shows more quantitatively that deviations from the total radiation behaviour predicted in this framework are significant mainly for $t \lesssim t_{th}$. The variation with time of the population of each vibrational level is shown in fig. 13 for the case $Z_{rot} = 10$ and in fig. 14 for $Z_{rot} = 0.2$. *We note that with the exception of narrow regions around thresholds the population of each vibrational level changes in a very smooth manner, essentially a steady-state behaviour.* For instance, the sudden drop in the population of $V = 2$ around 2.5 μs is due to the onset of radiation from that level (which is pos-

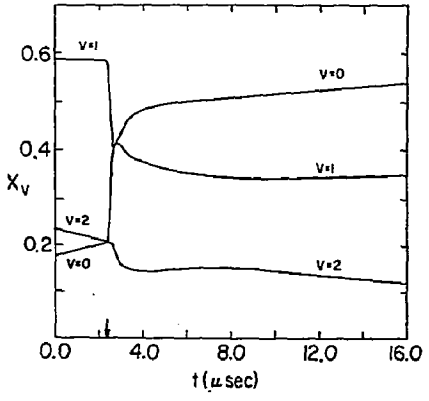

Fig. 13. Variation with time of the vibrational populations (for $V = 0$, $V = 1$, $V = 2$) – the case $Z_{rot} = 10$.

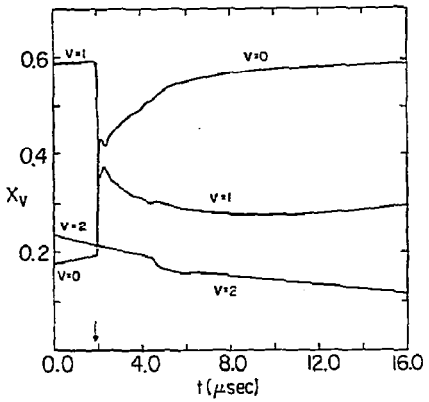

Fig. 14. Variation with time of the vibrational populations – the case $Z_{rot} = 0.2$.

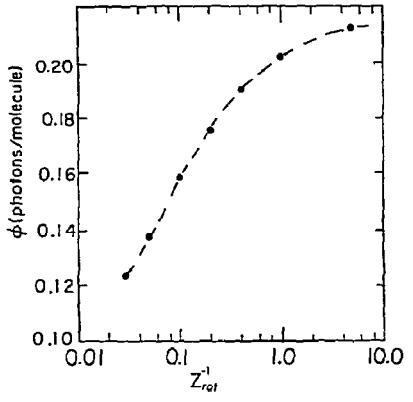

Fig. 15. Laser efficiency as function of rotational relaxation rate, Z_{rot}^{-1}. ϕ is the average number of photons extracted from one HCl molecule during the laser pulse.

sible for $Z_{rot} = 10$). The case of high R–T, fig. 14, shows a more extended transient region around threshold, and some structure due to relaxation oscillations can be seen. This is in agreement with the conclusion of previous sub-sections that the oscillatory domain becomes more extended and the amplitudes of the undulation increase as Z_{rot} decreases. But even for $Z_{rot} = 0.2$ for $t > t_{th}$ the behaviour of X_V is a steady-state one. Also for $t \gg t_{th}$ the differences between figs. 13 and 14, become small, i.e., the dependence of X_V upon Z_{rot} is weak. We conclude that quantities that are integrated with respect to rotational states show much smaller sensitivity to rotational non-equilibrium effects than individual vib-rotational variables. The strongest manifestations of rotational non-equilibrium in the properties of such integral quantities are in the threshold region and the efficiency.

4.3.5. Rotational non-equilibrium and laser efficiency

Inspection of figs. 13 and 14 shows that most of the laser radiation is extracted from partially inverted populations. The total output energy increases with Z_{rot}^{-1}, as reflected by the lower final value of X_1/X_0 in fig. 14 ($Z_{rot}^{-1} = 0.2$) in comparison to fig. 13 ($Z_{rot}^{-1} = 10$). This trend is confirmed more systematically in fig. 15 which displays the efficiency ϕ (number of output photons per HCl molecule) as function of Z_{rot}^{-1}. The more efficient extraction of laser energy at higher R–T rates should be attributed to the increasing influence of the funneling mechanism. As the R–T rate increases neighbouring P-branch transitions are more effectively coupled. Thus when a certain transition, say $J-1 \rightarrow J$, ceases to lase because J falls below J^* (see section 4) the upper vibrational level population can still be funneled 'downwards' due to stimulated emission through $J \rightarrow J+1$ and so on. When R–T transfer is slow adjacent transitions do not communicate and lasing terminates independently in every transition. That funneling allows

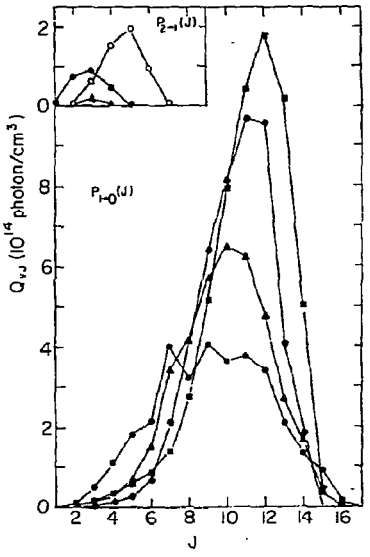

Fig. 16. Spectral distribution of laser output (integrated over time). $Z_{rot} = 0.2$ (■), 2.5 (♦), 10 (△), 33 (●), 10, all vibrational relaxation omitted (○) The graph in the upper part gives radiation from $V = 2$ (enlarged ten-fold).

more radiation to be extracted from lower values of X_1/X_0 and consequently higher values of J is illustrated also in fig. 16. This figure shows the (time) integrated spectral distribution of the laser output. The appearance of lasing in the $2 \rightarrow 1$ band at low Z_{rot}^{-1} values is due to the slow build-up of the Boltzmann peak in $V=1$, cf. fig. 1.

4.4. Contributions of various relaxation processes

The contributions of the various kinetic processes to the rate of change of a representative vib-rotational level are shown in fig. 17. In the early stages of the pulse relaxation processes are relatively unimportant and the vib-rotational populations are governed by the pumping and the stimulated emission. Vibrational relaxation (V–V and V–T) becomes influential when the concentration of lasing molecules reaches appreciable values. Vibrational relaxation causes quenching of the pulse when its rate exceeds the pumping rate. The 'hole filling tendency' of the R–T processes is clearly demonstrated in the pulse peak region; molecules from adjacent rotational levels flow into the hole burnt by the radiation thus giving rise to a positive contribution to $N_{V,J}$.

5. Concluding remarks

For an overall perspective of the insight gained by the computer experiments we repeat below in a condensed form some of the main results described in the previous section. We emphasize conclusions that may be of relevance to the interpretation of future ('real') experiments and for the development of models or approximate theoreis of laser kinetics.

(1) At low pressures the rotational distribution functions for both $V=1$ and $V=0$ differs substantially from the Boltzmann form during the laser pulse.

(2) Single line operation is a nearly correct description when, and only when, rotational equilibrium holds.

(3) The influence of rotational non-equilibrium on the behaviour of detailed vib-rotational variables (such as $N_{V,J}$ and $\rho_{V,J}$) is very large. Integrated quantities such as the fractional vibrational populations or the total radiation density are affected to a lesser extent.

(4) The fractional vibrational populations obey, to a good approximation, a steady-state behaviour outside the threshold regime.

(5) For low J's rotational relaxation at 'normal' pressures seems fast enough to ensure rotational thermalization. Positions of peaks calculated on the basis of this assumption are almost exact.

(6) Pulses at higher J's show an increased steady-state behaviour. The oscillation region is relatively small.

(7) Threshold oscillations are sensitive to the magnitude of the R–T rates.

(8) Laser efficiencies increase with R–T rates. Indicating that funneling is an efficient mechanism for extraction of radiation from partially inverted (high-J) levels.

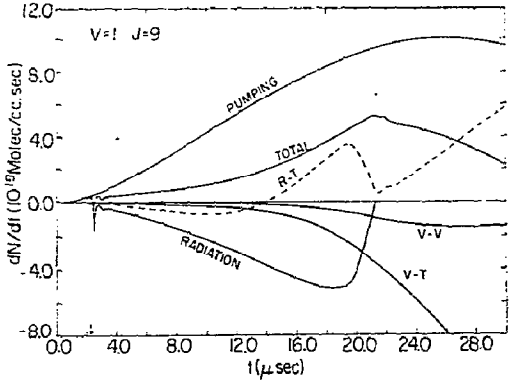

Fig. 17. Contribution of various processes to the rate of change of a representative vib-rotational population.

Acknowledgement

We would like to thank Professor A. Ben-Reuven for many helpful discussions and Dr. M. Baer for helpfull suggestions. We also thank Dr. P. Brumer for making one of his programmes available.

References

[1] B.F. Gordiets, A.I. Osipov, E.V. Stupeckenko and L.A. Shelepin, Soviet Physics Uspekhi 15 (1973) 759.
[2] J.R. Airey, J. Chem. Phys. 52 (1970) 156.
[3] N. Cohen, T.A. Jacobs, G. Emanuel and R.L. Wilkins, Int. J. Chem. Kinet. 1 (1969) 551.
[4] R.L. Kerber, G. Emanuel and J.S. Whittier, Appl. Optics 11 (1972) 1112.
[5] S.N. Suchard, R.L. Kerber, G. Emanuel and J.S. Whittier, J. Chem. Phys. 57 (1972) 5065.

[6] M.J. Molina and G.C. Pimentel, IEEE J. Quant. Elec., QE-9 (1973) 64.
[7] M.J. Berry, in: Molecular Energy Transfer, eds. R.D. Levine and J. Jortner (Wiley, New York, 1975).
[8] M.J. Berry, Ann. Rev. Phys. Chem. 26 (1975) xxx.
[9] T.D. Padrick and M.A. Gusinow, Chem. Phys. Lett. 24 (1974) 270.
[10] H.L. Chen, R.L. Taylor, J. Wilson, P. Lewis and W. Fyfe, J. Chem. Phys. 61 (1974) 306.
[11] H. Pummer and K.L. Kompa, Appl. Phys. Lett. 9 (1972) 356.
[12] A. Ben-Shaul, G.L. Hofacker and K.L. Kompa, J. Chem. Phys. 59 (1973) 4664.
[13] A. Ben-Shaul, O. Kafri and R.D. Levine, Chem. Phys. 10 (1975) 367.
[14] A. Ben-Shaul, K.L. Kompa and U.S. Schmailzl, J. Chem. Phys. 65 (1976) 1711.
[15] L.H. Sentman, J. Chem. Phys. 62 (1975) 3523.
[16] K.L. Kompa, Topics Curr. Chem. 37 (1973) 1.
[17] A.N. Chester and L.D. Hess, IEEE J. Quant. Elec., QE-8 (1972) 1.
[18] R. Herman and R.F. Wallis, J. Chem. Phys. 23 (1955) 637;
R. Herman, R.W. Rotheny and R.J. Rubin, J. Mol. Spectr. 2 (1958) 369.
[19] J.M. Herbelin and G. Emanuel, J. Chem. Phys. 60 (1974) 689.
[20] D.H. Maylotte, J.C. Polanyi and K.B. Woodall, J. Chem. Phys. 57 (1972) 1547.
[21] J.C. Polanyi and K.B. Woodall, J. Chem. Phys. 56 (1972) 1563.
[22] F.J. Wodarczyk and C.B. Moore, Chem. Phys. Lett. 26 (1974) 484;
K. Bergmann and C.B. Moore, J. Chem. Phys. 63 (1975) 643.
[23] S. Leone, R. MecDonald and C. Bradley Moore, J. Chem. Phys. 63 (1975) 4735. This article appeared after the work presented here had been completed. The authors propose the reactive deactivation is more significant than the V–T, but state that this is still speculative.
[24] C.B. Moore, Adv. Chem. Phys. 23 (1973) 41.
[25] B.M. Hopkins and H.L. Chen, J. Chem. Phys. 57 (1972) 3816.
[26] S.R. Leone and C.B. Moore, Chem. Phys. Lett. 19 (1973) 340.
[27] B.A. Ridley and I.W.M. Smith, Trans. Faraday Soc. 68 (1972) 1231.
[28] Y. Noter, I. Burak and A. Szöke, J. Chem. Phys. 59 (1973) 970.
[29] R.D. Sharma and C.A. Brau, J. Chem. Phys. 50 (1969) 924.
[30] T.A. Dillon,and J.C. Stephenson, J. Chem. Phys. 58 (1973) 2056.
[31] H.L. Chen and C.B. Moore, J. Chem. Phys. 54 (1971) 4080.
[32] S. Ormonde, Rev. Mod. Phys. 47 (1975) 193, and references therein.
[33] N.C. Craig and C.B. Moore, J. Phys. Chem. 75 (1971) 1622.
[34] D. Arnoldi, K. Kaufmann and J. Wolfrum, Phys. Rev. Lett. 34 (1975) 1597.
[35] J.M. White and D.L. Thompson, J. Chem. Phys. 61 (1974) 719.
[36] R.L. Wilkins, J. Chem. Phys. 63 (1975) 534.
[37] R.G. McDonald, C.B. Moore, I.W.M. Smith and F.J. Wodarczyk, J. Chem. Phys. 62 (1975) 2934.
[38] I.W.M. Smith and P.M. Wood, Mol. Phys. 25 (1973) 441.
[39] D.L. Thompson, J. Chem. Phys. 56 (1972) 3570.
[40] B.A. Ridley and I.W.M. Smith, Chem. Phys. Lett. 9 (1971) 457.
[41] A.M.G. Dign and J.C. Polanyi, Chem. Phys. 10 (1975) 39.
[42] P.M. Agrawal and M.P. Saksena, J. Chem. Phys. 61 (1974) 848.
[43] C.W. Gear. Numerical Initial Value Problems in Ordinary Differential Equations (Prentice–Hall, N.J. 1971).
[44] C.W. Gear, J. Siam. Num. Anal. 14 (1965). 69.
[45] P. Brumer, J. Computational Phys. 14 (1974) 391.
[46] M.J. Berry, J. Chem. Phys. 59 (1973) 6229.
[47] J.C. Polanyi, Appl. Optics Supp. 2 (1965) 109.
[48] I. Procaccia, Y. Shimoni and R.D. Levine, J. Chem. Phys. 63 (1975) 3181.
[49] H.G. Unger, Introduction to Quantum Electronics (Pergamon Press, Oxford, 1970).
[50] E. Keren, R.B. Gerber and A. Ben-Shaul, to be published.